Influence of coupling asymmetry on signal amplification in a three-node motif

Xiaoming Liang(梁晓明)[1,†], Chao Fang(方超)[1], Xiyun Zhang(张希昀)[2], and Huaping Lü(吕华平)[1]

[1] *School of Physics and Electronic Engineering, Jiangsu Normal University, Xuzhou* 221116, *China*
[2] *Department of Physics, Jinan University, Guangzhou* 510632, *China*

(Received 5 July 2022; revised manuscript received 2 September 2022; accepted manuscript online 21 September 2022)

The three-node feedforward motif has been revealed to function as a weak signal amplifier. In this motif, two nodes (input nodes) receive a weak input signal and send it unidirectionally to the third node (output node). Here, we change the motif's unidirectional couplings (feedforward) to bidirectional couplings (feedforward and feedback working together). We find that a small asymmetric coupling, in which the feedforward effect is stronger than the feedback effect, may enable the three-node motif to go through two distinct dynamic transitions, giving rise to a double resonant signal response. We present an analytical description of the double resonance, which agrees with the numerical findings.

Keywords: network motif, synchronization, coupling asymmetry, signal amplification

PACS: 05.45.Xt, 87.19.ln **DOI:** 10.1088/1674-1056/ac9363

1. Introduction

Designing an artificial structure that reproduces biological systems' signal processing capabilities is challenging.[1–5] Considerable progress has been achieved in this direction.[6–10] One-way chains are the early proposed signal amplification structures in which the first site receives an input signal, and the last site outputs it.[11–13] With suitable noise and coupling strength, one-way chains can boost weak signals. Later, two-dimensional arrays were found to exhibit a similar noise-boosted amplification effect.[14,15] However, regular arrays are idealized coupling designs since most natural systems, especially neural networks, have complex structures.[16–23] Successive studies have shown that network structure significantly affects the signal amplification function.[24–27] For instance, small-world networks with long-range links may improve the network response to a weak input;[28,29] scale-free networks with star structures can generate a double resonance at the hub and leaf nodes.[30,31]

In addition to small-world and scale-free global features, many networks also exhibit local motif properties.[32,33] That is, some small subgraphs appear more often than in random networks. The three-node motifs with thirteen possible configurations are well-known network motifs in biological organisms ranging from bacteria and yeast to animals.[33–35] Thus, it is interesting to investigate the specific signal processing functions each motif can perform. To this end, Guo *et al*. studied the stochastic resonance in three-neuron feedforward motifs. They found that noise and coupling strength are two parameters that control the sensitivity and reliability of the motifs' responses to external signals.[36] Liang *et al*. reported that the feed-forward motif with two uncoupled input nodes and one output node has a specific function in regulating signal propagation.[37,38] This signal regulation effect is also observed in a three-node motif in which two input neurons have interactions.[39]

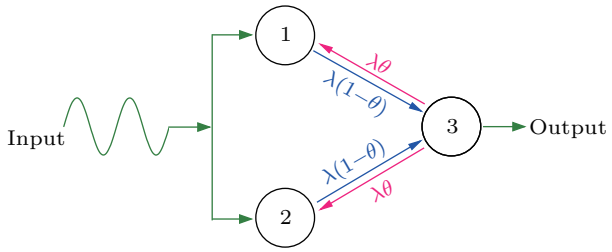


Fig. 1. A sketch of three-node motif with bidirectional couplings, where node 1 and node 2 receive the input signal and node 3 outputs the signal. When the coupling asymmetry parameter $\theta = 0$, this motif returns to the feedforward motif.

Following this motivation, we study the signal amplification in a three-node motif with bidirectional couplings between the input and the output nodes. Specifically, we introduce a parameter θ to represent the coupling asymmetry.[11,40] When $\theta = 0.5$, the couplings are symmetrical; when $\theta < 0.5$, the couplings from the input nodes to the output node are stronger than vice versa. Thus, the motif returns to the feedforward motif with directional couplings when $\theta = 0$ [see Fig. 1]. We find that when θ is small but nonzero, *i.e*., the output node feeds back a small influence on the input nodes, the signal response of the motif is amplified, and the coupling interval for signal amplification is expanded, displaying a double resonant signal response. We show that the asymmetrical coupling structure due to small feedback allows the motif to go through two distinct synchronization transitions, resulting in double resonance. We finally give a theoretical analysis to confirm our numerical results. We hope these findings will contribute

†Corresponding author. E-mail: xmliang@jsnu.edu.cn
© 2023 Chinese Physical Society and IOP Publishing Ltd

to a deeper understanding of the relationship between motif structure and signal processing functions.

2. Model

We start with the overdamped bistable oscillator with a double-well potential, which is often used as a baseline model for signal amplification.[41–44] The motif of three bistable oscillators has the following form:

$$\begin{aligned}\dot{x}_1 &= x_1 - x_1^3 + \lambda\theta(x_3 - x_1) + A\sin(\omega t),\\ \dot{x}_2 &= x_2 - x_2^3 + \lambda\theta(x_3 - x_2) + A\sin(\omega t),\\ \dot{x}_3 &= x_3 - x_3^3 + \lambda(1-\theta)(x_1 + x_2 - 2x_3),\end{aligned} \tag{1}$$

where λ is the coupling strength, and θ is a parameter describing the coupling asymmetry between nodes. Therefore, $\theta = 0$ and $\theta = 1$ represent two different unidirectional coupling configurations. Depending on the periodic input signal $A\sin(\omega t)$, individual oscillators ($\lambda = 0$) either vibrate in one potential well or switch between the wells. The transition from one-well vibration to well-to-well oscillation occurs at $A_c = \sqrt{4/27}$.[41] Without losing generality, we consider a subthreshold signal of $\omega = \pi/50$ and $A = 0.1 < A_c$ throughout our investigation.

For simplicity, we measure the signal response of the motif using the amplitude of the output node[24,25]

$$G = \frac{\max x_3 - \min x_3}{2A}. \tag{2}$$

Thus, if $G < 1$, the motif attenuates the input signal while amplifying it if $G > 1$. In addition, we quantify the spatial synchronization of the motif using the order parameter[45,46]

$$\rho = \frac{|n_+ - n_-|}{N}, \tag{3}$$

where n_+ and n_- are the number of oscillators in the positive well at $x_s = 1$ and the negative well at $x_s = -1$, respectively. Here $x_s = \pm 1$ are two stable fixed point of the overdamped bistable oscillator. When $\rho = 0$, the motif is asynchronous, with two nodes vibrating in the positive and negative potential wells and the third switching between them. When $\rho = 1$, the motif is synchronous, and all three nodes vibrate in the same well.

In numerical simulations, the initial states of the three nodes are chosen from $x_s = \pm 1$, where two input nodes are assigned with opposite signs to facilitate signal amplification, *i.e.*, $x_1(0) = -x_2(0)$.[37,38]

3. Simulations

In Fig. 2(a), we show the signal response of Eq. (1) as a function of the coupling strength for different coupling asymmetries. At $\theta = 0$, the motif generates a resonance-like signal amplification ($G > 1$) for intermediate coupling strength λ, consistent with the findings in Refs. [38,39]. As the coupling asymmetry increases to $\theta = 0.1$, the motif produces a double resonance, with the first resonance occurring at a small coupling strength λ_{c1} as in the case of $\theta = 0$, and the second resonance occurring at a relatively large coupling strength λ_{c2}. The signal response within the coupling interval $(\lambda_{c1}, \lambda_{c2})$ is greater than $\theta = 0$. Continuing to increase the coupling asymmetry to $\theta = 0.2$, the two resonance peaks slightly rise while the coupling interval between the double resonance peaks significantly shrinks. However, further increasing the coupling asymmetry (*e.g.*, $\theta = 0.4$) will eliminate the double resonance effect and return to the single resonance with a damped signal response ($G < 1$). Therefore, small feedback ($\theta \neq 0$) from the output node to the input nodes may optimize the signal amplification of the feedforward motif ($\theta = 0$). Meanwhile, figure 2(b) plots the spatial synchronization corresponding to the signal amplification as described in Fig. 2(a). In the case $\theta = 0$, the order parameter drops from $\rho = 1/3$ to $\rho = 0$ as the coupling strength λ exceeds λ_{c1}, suggesting that the resonance appearing at λ_{c1} is induced by a synchronization–asynchronization transition. In the presence of coupling asymmetry $\theta = 0.1$ and $\theta = 0.2$, the order parameter drops to $\rho = 0$ at λ_{c1}, similar to that of $\theta = 0$; but after that point it jumps to $\rho = 1$ at λ_{c2}. This jump indicates that the second resonance at λ_{c2} arises from an asynchronization–synchronization transition. However, the order parameter directly transits from $\rho = 0$ to $\rho = 1$ at λ_{c1} for the large coupling asymmetry $\theta = 0.4$, indicating that high levels of synchronization harm signal amplification.

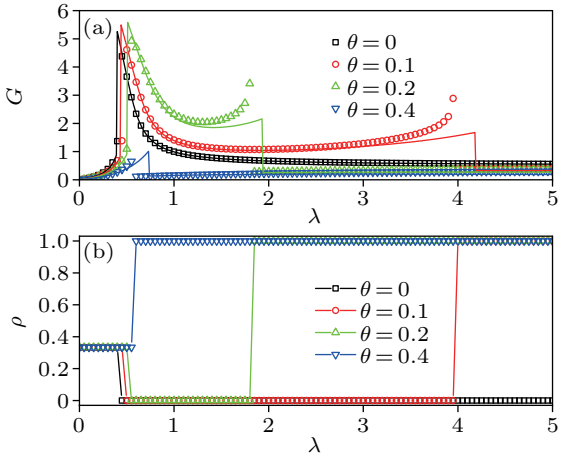


Fig. 2. Signal response G in panel (a) and order parameter ρ in panel (b) as a function of the coupling strength λ for coupling asymmetry $\theta = 0$, 0.1, 0.2, and 0.4. Dashed lines in panel (a) denote the predictions of Eq. (20).

In Fig. 3(a), we present the signal response for different pairs of coupling strength and the coupling asymmetry. For a better comparison, we normalize the signal response by dividing its value at $\theta = 0$, *i.e.*, $G' = G(\theta)/G(\theta = 0)$. As a result, $G' > 1$ means that the output node's feedback ($\theta > 0$) enhances the signal amplification. As seen in Fig. 3(a), the signal response $G' > 1$ emerges when the coupling strength and

the coupling asymmetry are over a pair of critical values θ_c and λ_c. In addition, there are two different relationships between θ_c and λ_c. Specifically, $\theta_c \sim \lambda_{c1}$ for small coupling strength and $\theta_c \sim \lambda_{c2}^{-1}$ for large coupling strength. That is, relatively large feedback may amplify the input signal for a small coupling strength, whereas small feedback may realize the signal amplification for a large coupling strength. Furthermore, figure 3(b) presents the order parameter corresponding to the signal response shown in Fig. 3(a). There are three regimes in the parameter space (θ,λ): partial synchronization with $\rho = 1/3$ (regime I), asynchronization with $\rho = 0$ (regime II), and synchronization with $\rho = 1$ (regime III). Clearly, regime II corresponds to the plateau with $G' > 1$ observed in Fig. 3(a), and its boundaries are exactly the relationships between θ_c and λ_{c1} and λ_{c2}.

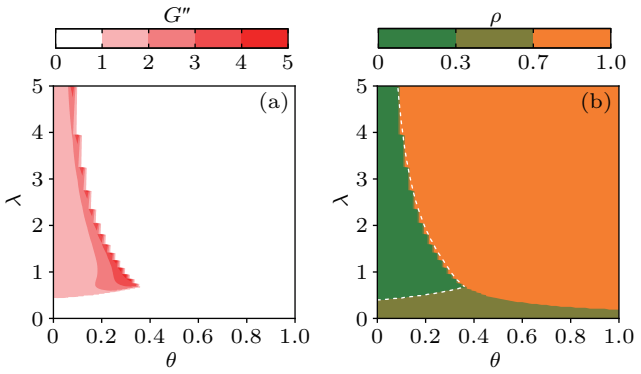


Fig. 3. Normalized signal response G' (a) and order parameter ρ (b) as a function of the coupling strength λ and the coupling asymmetry θ. Dashed lines in panel (b) denote the predictions of Eqs. (10) and (15).

4. Analysis

Denoting the average activity $y = (x_1 + x_2)/2$ and synchronization error $z = (x_1 - x_2)/2$ of the two input nodes, equation (1) turns into

$$\dot{y} = \left(1 - 3z^2 - \lambda\theta\right) y - y^3 + \theta\lambda x_3 + A\sin(\omega t), \tag{4}$$

$$\dot{z} = \left(1 - 3y^2 - \lambda\theta\right) z - z^3, \tag{5}$$

$$\dot{x}_3 = (1 - 2\lambda(1-\theta))\, x_3 - x_3^3 + 2\lambda(1-\theta) y. \tag{6}$$

Because the input nodes are driven by the same force, the amplitude of the synchronization error is much smaller than the average. Accordingly, we may assume $\dot{z} = 0$ and get $z^2 = 1 - 3y^2 - \theta\lambda$ and $z = 0$ from Eq. (5). These two distinct solutions correspond to asynchronization ($\lambda < \lambda_{c2}$) and synchronization ($\lambda \geq \lambda_{c2}$) of the two input nodes, respectively.

In the case of asynchronization ($z^2 = 1 - 3y^2 - \theta\lambda$), equation (4) simplifies to

$$\dot{y} = -2(1 - \lambda\theta) y + 8y^3 + \lambda\theta x_3 + A\sin(\omega t). \tag{7}$$

Similarly, we may assume $\dot{y} = 0$ and $8y^3 = 0$ since y is small and less than x_3 when $\lambda \ll \lambda_{c2}$. Then equation (7) becomes

$$y(t) = \frac{\lambda\theta x_3}{2(1-\lambda\theta)} + \frac{1}{2(1-\lambda\theta)} A\sin(\omega t). \tag{8}$$

Substituting it into Eq. (6) yields

$$\dot{x}_3 = \alpha x_3 - x_3^3 + \beta A\sin(\omega t), \tag{9}$$

where $\alpha = \lambda\left((1-\theta)(3\lambda\theta - 2) + (1 - \lambda\theta)\right)/(1 - \lambda\theta)$ and $\beta = \lambda(1-\theta)/(1-\lambda\theta)$. When $A = 0$, equation (9) has two stable fixed points $x_3^* = \pm\sqrt{\alpha}$ for $\alpha > 0$ and one stable fixed point $x_3^* = 0$ for $\alpha < 0$. Let λ_0 be the critical coupling strength for $\alpha = 0$. When $A \neq 0$, the periodic signal $\beta A\sin(\omega t)$ transits from subthreshold to suprathreshold if the coupling strength exceeds a critical value λ'_{c1} satisfying

$$\left(\frac{\beta A}{2}\right)^2 = \left(\frac{\alpha}{3}\right)^3. \tag{10}$$

As Fig. 2(a) shows, the critical λ'_{c1} of Eq. (10) fits the numerical data λ_{c1}. Since the periodic signal remains subthreshold for $\lambda < \lambda'_{c1}$, the output node will vibrate about $x_3^* = \pm\sqrt{\alpha}$, and its approximate solution can be derived using the linearization method as

$$x_3(t) = \pm\sqrt{\alpha} + \frac{\beta A}{\sqrt{\omega^2 + 4\alpha^2}}\sin(\omega t + \phi_1), \tag{11}$$

where $\phi_1 = \arctan(\omega/2\alpha)$ is the phase shift. For $\lambda \geq \lambda'_{c1}$, the periodic signal is suprathreshold which forces the output node to oscillate around $x_3^* = 0$. In this situation, the approximate solution of Eq. (9) is as follows: assuming the periodic signal as constants $\pm\beta A$ due to short ω,

(i) when $\alpha > 0$, *i.e.*, $\lambda < \lambda_0$,

$$x_3(t) = 2\left(\frac{\alpha}{3}\right)^{1/2}\cosh\left(\frac{\psi}{3}\right)\sin(\omega t), \tag{12}$$

where $\psi = \cosh^{-1}\left((3/\alpha)^{3/2} A\beta/2\right)$;

(ii) when $\alpha \leq 0$, *i.e.*, $\lambda \geq \lambda_0$,

$$x_3(t) = 2\left(-\frac{\alpha}{3}\right)^{1/2}\sinh\left(\frac{\psi}{3}\right)\sin(\omega t), \tag{13}$$

where $\psi = \sinh^{-1}\left((-3/\alpha)^{3/2} A\beta/2\right)$.

In the case of synchronization ($z = 0$), the three nodes vibrate in the same potential well. To obtain the analytical coupling strength λ'_{c2} for motif synchronization, we put Eq. (13) into Eq. (7) and find

$$\begin{aligned}\dot{y} = {} & -2(1 - \theta\lambda) y + 8y^3 \\ & + \left(2\theta\lambda\left(-\frac{\alpha}{3}\right)^{1/2}\sinh\left(\frac{\psi}{3}\right) + A\right)\sin(\omega t).\end{aligned} \tag{14}$$

According to Eq. (14), the average activity y oscillates about the stable fixed point $y^* = 0$ under a subthreshold force while it diverges under a suprathreshold force.[47] This is because Eq. (14) is derived from the asynchronization condition $z^2 = 1 - 3y^2 - \theta\lambda$; when $\lambda \geq \lambda'_{c2}$, the asynchronization condition is no longer satisfied and thus equation (14) becomes incorrect (divergence). Following Eq. (10), the coupling strength

λ'_{c2} for the signal in Eq. (14) changing from subthreshold to suprathreshold satisfies

$$\left(\frac{2\lambda'_{c2}\theta\,(-\alpha/3)^{1/2}\sinh(\psi/3)+A}{2}\right)^2=\left(\frac{1-\lambda'_{c2}\theta}{12}\right)^3. \quad (15)$$

Figure 2(a) shows the estimations of Eq. (15), which are slightly bigger than the numerical values λ_{c2}. The reason for this is that when the coupling strength approaches λ_{c2}, the motif tends to synchronize, *i.e.*, $y=x_3$, so the approximations of $\dot{y}=0$ and $8y^3=0$ are inaccurate in Eq. (7), giving rise to the large analytical λ'_{c2}.

Next, we substitute $z=0$ into Eq. (4) to obtain the average activity y for $\lambda\geq\lambda'_{c2}$, which takes the form

$$\dot{y}=(1-\lambda\theta)y-y^3+\lambda\theta x_3+A\sin(\omega t). \quad (16)$$

When the three nodes are in one well, the value of x_3 is smaller than y since the output node has no external periodic drive signal. For this reason, we may suppose $x_3=\pm1$ in Eq. (16) and obtain the approximate solution of the average activity y as

$$y(t)=\pm1+\frac{A}{\sqrt{\omega^2+(2+\lambda\theta)^2}}\sin(\omega t+\phi_2), \quad (17)$$

where $\phi_2=\arctan(\omega/(2+\lambda\theta))$ is the phase shift. Putting Eq. (17) into Eq. (6) gives

$$\begin{aligned}\dot{x}_3 &= \pm2\lambda(1-\theta)+(1-2\lambda(1-\theta))x_3-x_3^3\\ &\quad+\frac{2\lambda(1-\theta)A}{\sqrt{\omega^2+(2+\lambda\theta)^2}}\sin(\omega t+\phi_2). \quad (18)\end{aligned}$$

Its approximated solution is

$$\begin{aligned}x_3(t) &= \pm1+\frac{2\lambda(1-\theta)A}{\sqrt{\omega^2+4(1+\lambda-\lambda\theta)^2}\sqrt{\omega^2+(2+\theta\lambda)^2}}\\ &\quad\times\sin(\omega t+\phi_3), \quad (19)\end{aligned}$$

where $\phi_3=\arctan(\omega/(1+\lambda-\lambda\theta))$ is the phase shift.

Combining Eqs. (11)–(13) and (19), we can obtain the analytical signal response of Eq. (1) as

$$G=\begin{cases}\dfrac{\beta}{\sqrt{\omega^2+4\alpha^2}}, & \text{if } \lambda<\lambda'_{c1},\\ \dfrac{2}{A}\left(\dfrac{\alpha}{3}\right)^{1/2}\cosh\left(\dfrac{\psi}{3}\right), & \text{if } \lambda'_{c1}\leq\lambda<\lambda_0,\\ \dfrac{2}{A}\left(-\dfrac{\alpha}{3}\right)^{1/2}\sinh\left(\dfrac{\psi}{3}\right), & \text{if } \lambda_0\leq\lambda<\lambda'_{c2},\\ \dfrac{I}{A}, & \text{if } \lambda'_{c2}\leq\lambda,\end{cases} \quad (20)$$

where I is the amplitude of Eq. (19). Figure 2(a) shows the analytical results of Eq. (20), which correctly predict the aforementioned double resonance. Note that the double resonance peaks are located at the dynamic transition points λ'_{c1} and λ'_{c2}. This can be explained as follows. The periodic signals in Eqs. (9) and (14) become suprathreshold at λ'_{c1} and λ'_{c2}. In the former case λ'_{c1}, the suprathreshold signal allows the output node to leave the potential well, decreasing the spatial synchronization. In the latter case λ'_{c2}, the suprathreshold signal drives the input nodes to synchronize with the output node, increasing the spatial synchronization. Both cases imply that the motif is very sensitive to external signals in the vicinity of the synchronization transition points.

5. Summary

In conclusion, we have studied the signal amplification in a three-node motif composed of overdamped bistable oscillators, focusing on the effect of asymmetrical couplings between the input and output nodes. We have shown that the motif may generate a double resonant response to a subthreshold signal when the couplings from the output node to the input nodes are weaker than *vice versa*. We have found that the asymmetrical coupling-induced double resonant signal response is higher than the single resonant signal response in the feedforward motif with only unidirectional couplings from the input nodes to the output node. We have revealed that two different spatial synchronization transitions account for the emergence of the double resonance in the asymmetrically coupled three-node motif. Motifs are the basic building blocks of complex networks. On the one hand, our findings contribute to the knowledge of the signal amplification mechanism of the three-node network motifs. On the other hand, they provide a simple yet instructive description of the network structure-function relationship.

Acknowledgment

Project supported by the National Natural Science Foundation of China (Grant Nos. 12175087 and 12105117).

References

[1] Samardak A, Nogaret A, Janson N B, Balanov A G, Farrer I and Ritchie D A 2009 *Phys. Rev. Lett.* **102** 226802
[2] Zhou J, Zhou Y and Liu Z 2011 *Phys. Rev. E* **83** 046107
[3] Jiang L, Lai L, Yu T and Luo M 2021 *Chin. Phys. B* **30** 060502
[4] Lillicrap T P, Santoro A, Marris L, Akerman C J and Hinton G 2020 *Nat. Rev. Neurosci.* **21** 335
[5] Yao Y 2021 *Chin. Phys. B* **30** 060503
[6] Gammaitoni L, Hänggi P, Jung P and Marchesoni F 1998 *Rev. Mod. Phys.* **70** 223
[7] Badzey R L and Mohanty P 2005 *Nature* **437** 995
[8] Kanki T, Hotta Y, Asakawa N, Kawai T and Tanaka H 2010 *Appl. Phys. Lett.* **96** 242108
[9] Karabalin R B, Lifshitz R, Cross M C, Matheny M H, Masmanidis S C and Roukes M L 2011 *Phys. Rev. Lett.* **106** 094102
[10] Peters K J H, Geng Z, Malmir K, Smith J M and Rodriguez S R K 2021 *Phys. Rev. Lett.* **126** 213901
[11] Zhang Y, Hu G and Gammaitoni L 1998 *Phys. Rev. E* **58** 2952
[12] Lü H and Hu G 2004 *Phys. Rev. E* **69** 036212
[13] Li Q and Lang X 2006 *Phys. Rev. E* **74** 031905
[14] Rousseau D, Duan F and Chapeau-Blondeau 2003 *Phys. Rev. E* **68** 031107

[15] Lindner J F, Chandramouli S, Bulsara A R, Löcher M and Ditto W L 1998 *Phys. Rev. Lett.* **81** 5048
[16] Barabási A L and Albert R 1999 *Science* **286** 509
[17] Strogatz S H 2001 *Nature* **410** 268
[18] Bullmore E and Sporns O 2009 *Nat. Rev. Neurosci.* **10** 186
[19] Wang Q, Perc M, Duan Z and Chen G 2009 *Phys. Rev. E* **80** 026206
[20] Zhang J, Hang S, Pang S, Wang M and Gao S 2015 *Chin. Phys. Lett.* **32** 120502
[21] Zhang X, Boccaletti S, Guan S and Liu Z 2015 *Phys. Rev. Lett.* **114** 038701
[22] Boccaletti S, Almendral J A, Guan S, Leyva I, Liu Z, Sendiña-Nadal I, Wang Z and Zou Y 2016 *Phys. Rep.* **660** 1
[23] Pan T, Huang X, Xu C and Lü H 2019 *Chin. Phys. B* **28** 120503
[24] Acebrón J A, Lozano S and Arenas A 2007 *Phys. Rev. Lett.* **99** 128701
[25] Kondo T, Liu Z and Munakata T 2010 *Phys. Rev. E* **81** 041115
[26] Chacón R and Martínez P J 2015 *Phys. Rev. E* **92** 012821
[27] Shen Q and Liu Z 2021 *Phys. Rev. E* **103** 052414
[28] Gao Z, Hu B and Hu G 2001 *Phys. Rev. E* **65** 016209
[29] Perc M 2007 *Phys. Rev. E* **76** 066203
[30] Perc M 2008 *Phys. Rev. E* **78** 036105
[31] Liu Z and Munakata T 2008 *Phys. Rev. E* **78** 046111
[32] Alon U 2007 *Nat. Rev. Genet.* **8** 450
[33] Milo R, Shen-Orr S, Itzkovitz S, Kashtan N, Chklovskii D and Alon U 2002 *Science* **298** 824
[34] McCullen N J, Mullin T and Golubitsky M 2007 *Phys. Rev. Lett.* **98** 254101
[35] Ushakov Y V, Dubkov A A and Spagnolo B 2011 *Phys. Rev. Lett.* **107** 108103
[36] Guo D and Li C 2009 *Phys. Rev. E* **79** 051921
[37] Liang X, Yanchuk S and Zhao L 2013 *Phys. Rev. E* **88** 012910
[38] Liang X, Tang M and Lü H 2013 *Chaos* **23** 043113
[39] Ding W, Gu C and Liang X 2016 *Commun. Theor. Phys.* **65** 189
[40] Bragard J, Boccaletti S and Mancini H 2003 *Phys. Rev. Lett.* **91** 064103
[41] Moss F, Pierson D and O'Gorman D 1994 *Int. J. Bifurcation Chaos Appl. Sci. Eng.* **4** 1383
[42] Pikovsky A, Zaikin A and de la Casa M A 2002 *Phys. Rev. Lett.* **88** 050601
[43] Tessone C J, Mirasso C R, Toral R and Gunton J D 2006 *Phys. Rev. Lett.* **97** 194101
[44] Wang Z and Liu Z 2021 *Chaos* **31** 063126
[45] Lu F and Liu Z 2009 *Chin. Phys. Lett.* **26** 040503
[46] Liang X and Zhang X 2021 *Phys. Rev. E* **104** 034204
[47] Liang X, Liu C and Zhang X 2020 *Phys. Rev. E* **101** 022205